Analysis and design aspects of delayed resonator absorber with position, velocity or acceleration feedback

Tomáš Vyhlídal [a,c] Dan Pilbauer [a,b] Baran Alikoc [c]
Wim Michiels [b]

[a] *Dept. of Instrumentation and Control Eng., Faculty of Mechanical Engineering, Czech Technical University in Prague, Technická 4, 166 07 Praha 6, Czech Republic,* Tomas.Vyhlidal@cvut.cz

[b] *Department of Computer Science, KU Leuven, Celestijnenlaan 200A, B-3001 Heverlee, Belgium,* Wim.Michiels@cs.kuleuven.be

[c] *Czech Institute of Informatics, Robotics and Cybernetics, Czech Technical University in Prague, Jugoslávských partyzánů 3, 160 00 Praha 6, Czech Republic,* Baran.Alikoc@cvut.cz

Abstract

A thorough analysis of six delayed resonator configurations is performed. Considering either lumped or distributed delays, feedback is taken from acceleration, velocity or position measurements. Next to presenting stability maps derived by the Cluster Treatment of Characteristic Roots, the robustness in the vibration suppression is analyzed. It is shown that the deterioration of vibration suppression caused by mismatch between the design and true excitation frequencies can be decreased by a proper selection of the delayed resonator configuration and the frequency operable range. Besides, the force and energy demands from the resonator feedback are studied with respect to the absorber physical parameters. All the results are derived for a dimensionless model form and as such they are universally valid. Thus, with respect to the important design specifications, the analysis is complete and can be used as guidelines for parametrization of the given delayed resonator set, with respect to the operable conditions.

Key words: active vibration control, delayed resonator, time delay system, stability, spectral method

19 April 2019

1 Introduction

The concept of delayed resonator (DR) was proposed in the 1990s by N. Olgac and his co-workers [1–16]. It belongs to the class of active vibration absorbers where the main objective is to enhance the efficiency and flexibility in vibration suppression compared to the passive absorbers. The positive impact of passive absorbers to vibration amplitude reduction has been known for decades, see e.g. [17, 18]. The benefits of the easy to apply passive approach, where the absorber is mechanically mounted on the platform to be damped, is the inherent stability of the overall set-up and robustness to mismatch between design and true excitation frequency. However, the frequency range where efficient vibration suppression takes place is relatively narrow, centered at the natural frequency of the absorber. Moreover, due to physical constraints, the passive absorber is never ideal (its damping is nonzero) and thus the vibrations are not damped entirely even if the vibration frequency is identical with the natural frequency of the absorber.

A passive absorber is turned to an active absorber (resonator) by including an active feedback with the two key objectives: i) to enhance the absorber characteristic towards ideal (full) vibration absorption at a given excitation frequency, and ii) to widen the frequency range on which the absorber can efficiently suppress the vibration via tuning the feedback parameters. However, this brings a number of problems to be solved, mainly concerning the stability of the overall structure and the robustness against parameter and frequency variation. Next to the DR approach, alternative methods for tuning the mechanical parameters of the absorber, particularly the stiffness of the dampers [17, 18], have been developed in order to extend applicable range of frequencies where the absorber is effective, see also [19] for broad-band damping tuned mass-damper design.

In Fig. 1, the overall DR set-up is depicted. It consists of an active vibration absorber (A), which is attached to the single degree-of-freedom primary structure (P). By properly tuned feedback, force $u(t)$ can enhance elimination of disturbing effects of harmonic oscillations $f(t)$ acting on the primary structure. The key objectives performed by the active feedback are given as follows:

(1) For a given excitation frequency $\bar{\omega}$, the feedback turns the physical absorber to an ideal resonator absorber which suppresses the vibrations entirely.
(2) The parameters of the feedback can be tuned with respect to the excitation frequency $\bar{\omega}$ variations.

The DR feedback can be implemented using delayed position, velocity or ac-

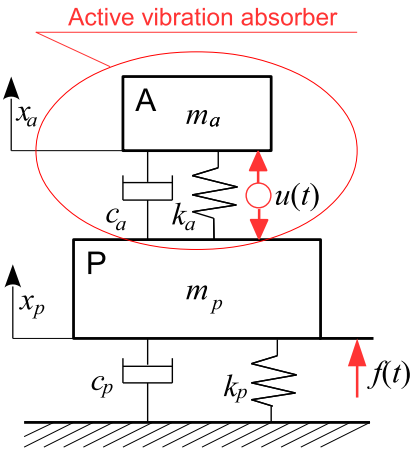

Fig. 1. Primary Structure (P), with an active vibration absorber (A) to suppress displacement x_p induced by harmonic disturbance force $f(t)$

celeration measurements, depending on the type of sensor selected for a particular vibration control application at hand. Note that the DR delay serves as one parameter to be tuned while the feedback gain is the other one. The DR concept was introduced in [1, 2, 5] utilizing position feedback, see also [6] for the design considerations. Subsequent modifications of the resonator concept include a single-mass dual frequency absorber [7], [8] or relative position feedback absorber [3]. In [9] and [10], the approach was extended to a centrifugal pendulum absorber. The analysis and design of the DR in discrete time domain was performed in [11]. Recently, a new venue for position DR-based vibration control using piezoelectric networks was proposed in [20].

In [4] the basic theory proposed for position feedback is modified for feedback with acceleration measurements and then experimentally validated. In the subsequent works on acceleration feedback based DRs, the robustness against uncertainties and variations in the parameters of the absorber arrangement was addressed by automatic tuning algorithms [12], [13]. The modal analysis of flexible beam with attached DR was performed in [21]. A multi degree-of-freedom structure with multiple DRs application is addressed in [14] where multiple absorbers are used to suppress different harmonics. The stability of the entire system is investigated using stability charts. The stability of the vibration absorber using acceleration and displacement feedback was derived in [22] utilizing the Nyquist criterion. Let us also point to a delay free alternative to the DR proposed in [23], which is based on filtered PI acceleration feedback. The author's team recently proposed a modified DR [24] where the acceleration based delayed feedback is extended by a non-delay path in order to widen the applicable vibration suppression frequency range. Another contribution of the authors' team is in the design of a robust DR by optimizing the delay distribution [25], see also [26]. DR velocity feedback was considered in [15] and [16] where it was applied and tuned for torsional vibration suppression. The velocity feedback was also considered in the recent application

with a modified delayed resonator for active suspension systems of railway vehicles [27]. A combination of delayed position and velocity feedback was considered in [28].

Recently, a complete dynamics analysis of a DR with acceleration feedback was performed in [29]. The analysis shows a negative effect when lumped-delayed feedback is taken from acceleration measurements, which results in undesirable neutral time delay system dynamics for both the resonator and its coupling with the primary structure. In order to mitigate this undesirable effect, an alternative distributed-delay resonator was proposed and analyzed in [30] resulting in retarded spectral properties, which are more convenient. The second benefit of this novel resonator scheme is that the distributed delay provides a filtering of the measured noise. By applying the method of *Cluster Treatment of Characteristic Roots* [31, 32], it was shown in [29] and [30] that for both the DRs, their operable frequency range is limited. From below, it is limited by the stability boundary, while the delay implementation aspects limit the range from the above - due to the fast decay of the delay length with respect to growing frequency. One of the key results presented in [29] and [30] are the stability maps of the delayed resonators. For a given damping of the resonator absorber, the operable frequency range under which the resonator is stable is provided.

Despite the thorough analysis of the various delayed resonator types, still, it cannot be considered as completed. Primarily, the force to be generated by the active resonator feedback and related energy demands for the entire vibration suppression have not been systematically addressed so far. These aspects are crucial for optimizing the absorber parameters and feedback actuator design. This missing analysis is performed in Section 3 as the first contribution of the paper, which follows after Section 2 containing the problem formulation and preliminaries. It will be shown that, interestingly, these characteristics are independent of the selected feedback type. Then, the thorough cross-comparison of parameter ranges of DRs with acceleration, velocity and position feedback and either lumped or distributed delay is performed in Section 4. Note that the distributed-delay DRs with position and velocity feedback are considered and designed for the first time here. Then, by adopting the methodology proposed in [29] and [30] the stability and, as an entirely novel contribution, also the robustness against mismatch between design and true excitation frequency are targeted in Section 5 for all the DR types. The key objective of this section is to analyze the applicability and effectiveness of the considered DR configurations. Finally, the application aspects for the active resonator absorber design are discussed in Section 6, which is followed by concluding remarks in Section 7.

2 Problem formulation and preliminaries

The dynamic model of the absorber is considered in the form

$$m_a \ddot{x}_a(\bar{t}) + c_a \dot{x}_a(\bar{t}) + k_a x_a(\bar{t}) = \bar{u}(\bar{t}), \tag{1}$$

with x_a being the displacement and $\bar{u}$ an external input force. The physical parameters of the absorber are m_a[kg], c_a[kgs^{-1}], k_a[Nm^{-1}] denoting the mass, damping and the stiffness. The time $\bar{t}$[s] is used to distinguish it from the dimensionless time t [−], which is scaled with respect to the natural frequency $\Omega = \sqrt{\frac{k_a}{m_a}}$ of the absorber (by $t = \bar{t}\Omega$). Scaling further the parameters of Equation (1) by the absorber mass m_a, and introducing the damping ratio parameter $\zeta = \frac{c_a}{2\sqrt{m_a k_a}}$, the absorber model (1) can be turned to the universal form

$$\ddot{x}_a(t) + 2\zeta \dot{x}_a(t) + x_a(t) = u(t), \tag{2}$$

with *dimensionless* parameters. Note that the absorber position x_a keeps the dimension [m] and the input is normalized

$$u = \frac{1}{m_a \Omega^2} \bar{u} \tag{3}$$

with dimension also [m]. This formal conversion simplifies the dynamic analysis of the delayed resonator - notice that equation (2) only has a single parameter ζ - and the results can be generalized to a full class of absorbers that can be described by the model (1).

The model of the absorber-primary coupling according to Fig. 1, considering the scaled parameters with respect to m_a and Ω, is given by

$$\ddot{x}_a(t) + 2\zeta \dot{x}_a(t) + x_a(t) - 2\zeta \dot{x}_p(t) - x_p(t) = u(t), \tag{4}$$

$$m_p \ddot{x}_p(t) + (2\zeta + c_p)\dot{x}_p(t) + (1 + k_p) x_p(t) - 2\zeta \dot{x}_a(t) - x_a(t) = -u(t) + f(t), \tag{5}$$

where $x_p(t)$ is the position and m_p, c_p, k_p are the scaled mass, the damping and the stiffness parameters of the primary structure, and $f(t)$ is the normalized periodic excitation force with normalized frequency $\omega = \frac{\bar{\omega}}{\Omega}$[−], where $\bar{\omega}$[s^{-1}] is the physical excitation frequency.

Consider the Laplace transforms of the variables $U(s) = \mathcal{L}\{u(t)\}$, $X_a(s) = \mathcal{L}\{x_a(t)\}$, $X_p(s) = \mathcal{L}\{x_p(t)\}$ and $F(s) = \mathcal{L}\{f(t)\}$. The absorber feedback to

suppress the vibration can be turned to the form

$$U(s) = P(s) X_a(s), \tag{6}$$

where $P(s)$ is the transfer function of the feedback. For the overall set-up (4)-(5), the transfer function between the excitation force f and the position of the platform with feedback (6) is given by

$$G_{x_p,f}(s) = \frac{R(s) - P(s)}{(R(s) - P(s))V(s) + (P(s) - Q(s))Q(s)} \tag{7}$$

with

$$R(s) = s^2 + 2\zeta s + 1 \tag{8}$$

being the characteristic function of the absorber (2), and $V(s) = m_p s^2 + (2\zeta + c_p)s + (1 + k_p)$, $Q(s) = 2\zeta s + 1$.

If the transfer function $P(s)$ is parameterized so that the characteristic equation of the resonator composed of the absorber (2) and the feedback (6), given by

$$M(s) = R(s) - P(s) = 0, \tag{9}$$

has a root couple $s_{1,2} := \pm j\omega$ composing a pole couple of the resonator, then

$$G_{x_p,f}(j\omega) = 0, \tag{10}$$

indicating that no vibrations at the given frequency ω are transferred in this f to x_p channel and the vibrations are ideally suppressed.

Note however, that including the resonator feedback affects the dynamical properties of the entire system, which is determined by the roots of the characteristic equation

$$(R(s) - P(s))V(s) + (P(s) - Q(s))Q(s) = 0. \tag{11}$$

Due to the presence of the delay terms in $P(s)$, Equation (11) has infinitely many roots. For the stability implications, all of them need to be located safely in the left half of the complex plane. Even though the root distribution of the characteristic equation of the resonator plays a fundamental role in distribution of high frequency roots of the characteristic equation of the closed loop system (11), see [29] and [30], the stability of the delayed resonator, determined by the roots of (9), is not necessary condition for functioning of the overall set-up. However, from the resonator implementation point of view, designing the resonator as stable (more precisely marginally stable due to roots assigned on the imaginary axis) is the crucial task. In real applications, one needs to consider the case when the position of the main platform is (temporally) fixed, e.g. due to effect of (strong) external disturbance or due to attaching the spring bumper. If not designed as (quasi)stable, the resonator

feedback would destabilize the absorber, which could result in its physical damage.

Another problem arising from the above described design of the delayed resonator is the robustness with respect to a mismatch between the true and nominal excitation frequencies. As will be shown, such a robustness highly depends on the parameters of the resonator absorber and the given operable range of frequencies. Thus the primary objective of the paper is to analyse the dependence of these two aspects i) stability, and ii) robustness, with respect to the absorber properties and the feedback type. We will consider a complete set of the resonator feedback, i.e. with acceleration, velocity and position measurements, and with both lumped and equally distributed delays. The presented research is targeted towards forming practical recommendations on resonator absorber design for a given operable frequency range. For this purpose, naturally, assessing the force and energy demands are also crucial aspects. As they are independent from the feedback type, they are studied first in the subsequent section.

3 Force amplitude and energy demands of resonator for vibration suppression

We provide new results on the resonator performance, taking into account the normalized force u exerted by the active control, as well as the amount of required normalized power, in the stationary regime induced by the periodic excitation force

$$f(t) = F\cos(\omega t). \tag{12}$$

In this stationary regime, the primary structure is considerred to be completely damped, i.e. $x_p = 0$. The only property of the designed resonator feedback we use is that $R(j\omega) - P(j\omega) = 0$. The following explicit expression for the force is obtained.

Proposition 1 *The stationary solution corresponding to the periodic excitation (12) is characterized by the periodic force*

$$u(t) = U\cos(\omega t - \phi), \tag{13}$$

with

$$U = \frac{F}{\omega^2}\sqrt{(1-\omega^2)^2 + 4\zeta^2\omega^2} \tag{14}$$

$$\phi = \begin{cases} \arcsin\left(\frac{2\zeta\omega}{\sqrt{(1-\omega^2)^2+4\zeta^2\omega^2}}\right), & \omega \geq 1, \\ \pi - \arcsin\left(\frac{2\zeta\omega}{\sqrt{(1-\omega^2)^2+4\zeta^2\omega^2}}\right), & \omega \leq 1. \end{cases} \tag{15}$$

Proof. In the stationary regime, all state variables are periodic functions of time and we can express

$$f(t) = \Re(Fe^{j\omega t}),\ u(t) = \Re(\mathcal{U}e^{j\omega t}),\ x_a(t) = \Re(\mathcal{X}_a e^{j\omega t}),$$

with $\mathcal{U}$ and $\mathcal{X}_a$ the complex amplitude of u and x_a, containing both magnitude and phase information. Furthermore, since the vibration of the primary structure is suppressed, we have $x_p \equiv 0$. Hence, we get from (4)

$$\mathcal{U} = (-\omega^2 + 2\zeta j\omega + 1)\mathcal{X}_a. \tag{16}$$

Similarly we get from (5) and (6)

$$(-2\zeta j\omega - 1 + P(j\omega))\mathcal{X}_a = F,$$

which taking into account $R(j\omega) - P(j\omega) = 0$ reduces to

$$-\omega^2\mathcal{X}_a = F. \tag{17}$$

By combining (16) and (17) we arrive at

$$\mathcal{U} = -\frac{F}{\omega^2}(1 - \omega^2 + 2\zeta j\omega)$$

Hence, we can write $u(t) = U\cos(\omega t - \phi)$ with $U = |\mathcal{U}|$ and $\phi = -\angle(\mathcal{U})$. □

Note from (17) that the amplitude of absorber stationary oscillations can directly be derived as

$$X_a = \frac{F}{\omega^2}, \tag{18}$$

which is also an important parameter for the physical absorber design. Interestingly, the amplitude is independent of the absorber damping ζ.

The amount of power needed for the active control of the DR does not only depend on the amplitude of the force but also on the phase with respect to the motion of the resonator. With excitation (12) the amount of power in stationary regime is time-periodic. Given that $x_p \equiv 0$ energy can only be transferred to and from the resonator. Hence the supplied power at time t is given by

$$P(t) = u(t)\dot{x}_a(t).$$

The averaged supplied power over the excitation period $T = 2\pi/\omega$ can be defined as

$$P_{\text{av}} = \frac{1}{T}\int_0^T u(t)\dot{x}_a(t)dt.$$

Proposition 2 *The stationary solution corresponding to excitation (12) is*

characterized by

$$P_{\text{av}} = \frac{F^2\zeta}{\omega^2}. \tag{19}$$

Moreover we have,

$$P(t) = P_{\text{av}} + \frac{F^2}{2\omega^3}\sqrt{(1-\omega^2)^2 + 4\zeta^2\omega^2}\,\sin(2\omega t - \phi), \tag{20}$$

with ϕ defined in (15).

Proof. We have $u(t) = U\cos(\omega t - \phi)$ as in Proposition 1 and from (17) we get

$$\dot{x}_a(t) = \frac{F}{\omega}\sin(\omega t).$$

Hence, by the Simpson formulas,

$$\begin{aligned} u(t)\dot{x}_a(t) &= \tfrac{FU}{\omega}\sin(\omega t)\cos(\omega t - \phi) \\ &= \tfrac{FU}{2\omega}\left(\sin(\phi) + \sin(2\omega t - \phi)\right). \end{aligned}$$

Hence

$$P_{\text{av}} = \frac{FU}{2\omega}\sin(\phi).$$

From the expression for ϕ in (15) we get

$$\sin\phi = \frac{2\zeta\omega}{\sqrt{(1-\omega^2)^2 + 4\zeta^2\omega^2}}$$

and taking into account the expression for U in (14) we arrive at (19)-(20). □.

Let us conclude by discussing the results of Propositions 1-2. The periodic force u in (13) is only determined by ζ and ω, *not* by the type of feedback considered. The amplitude of this force is zero if $\omega = 1,\ \zeta = 0$, and nonzero otherwise. Indeed, one may need the active feedback for two purposes: i) to change the damping ratio of the passive resonator to zero, and ii) to change its natural frequency to ω. However, as (19) expresses, only a *net* injection of energy over a cycle is needed when ζ is nonzero, in order to compensate the losses induced by the damping.

If one only needs to correct the frequency, this can be done with purely "reactive" power (90 degree phase shift between force and velocity). This fact has a physical explanation: in the absence of damping the passive resonator cannot loose energy, while an accumulation of energy is impossible due to the stationarity of the periodic regime. Note from (20) that in such a case the power P is a sinusoidal function with zero mean, characterized by balanced phases of energy supply and extraction.

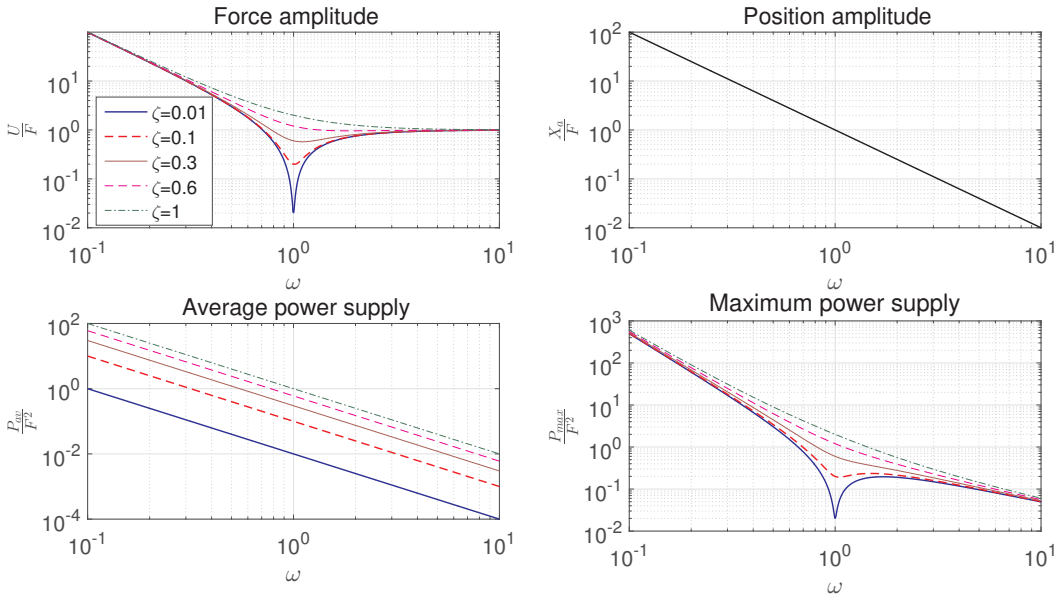

Fig. 2. Normalized amplitudes of the force U, average power supply P_{av} and maximum power supply $P_{\max}$ for various values of damping ζ, and normalized amplitude of the absorber position X_a.

In all cases, the maximum value of P corresponds to energy supply. It is given by

$$P_{\max} = \frac{F^2\zeta}{\omega^2} + \frac{F^2}{2\omega^3}\sqrt{(1-\omega^2)^2 + 4\zeta^2\omega^2}. \tag{21}$$

The graphical summary of the performed analysis is shown in Fig. 2. Concerning the actuator design, the main quantities are the force amplitude U and position amplitude X_a corresponding to the excitation force amplitude F. Even though the value of normalized force $\frac{U}{F}$ depends substantially on the damping parameter ζ close to $\omega = 1$, the dependency tends to diminish for both increasing and decreasing frequencies. The position amplitude is entirely independent of the damping ratio ζ. Thus, when designing the force actuator of the resonator, the absorber damping ζ is not the crucial parameter. This is however not the case from the energy consumption point of view, from which the absorbers with minimal damping should be preferred.

4 Resonators with lumped and distributed delay feedback

We consider resonator feedback with both lumped delay

$$u(t) = g y_a(t-\tau), \tag{22}$$

and equally distributed delay

$$u(t) = g\frac{1}{\tau}\int_0^{\tau} y_a(t-\theta)d\theta, \tag{23}$$

assuming the measured output y_a can be acceleration, $y_a = \ddot{x}_a$, velocity, $y_a = \dot{x}_a$ or position, $y_a = x_a$. Note that the benefit of the distributed delay is that it acts as a moving average filter and removes the undesirable neutrality for the case of acceleration feedback [30]. The parameters to tune are the gain g and the delay τ, which both depend on the feedback configuration.

The transfer function of the resonator feedback can be written in the following generic form

$$P(s, g, \tau) = \frac{X_a(s)}{U(s)} = gD(s, \tau)s^q, \tag{24}$$

where $D(s, \tau)$ is the transfer function of the delay term, which is given by

$$D(s, \tau) = e^{-s\tau} \tag{25}$$

for the lumped, and

$$D(s, \tau) = \frac{1 - e^{-s\tau}}{\tau s} \tag{26}$$

for the distributed delay. The parameter q then depends on the output type, i.e. it is $q = 0$ for position, $q = 1$ for velocity and $q = 2$ for acceleration measurements.

As mentioned in the preliminaries, the tuning of parameters g and τ is done by assigning a root $s_1 = j\omega$ to the characteristic equation (9). The resulting feedback forms and tuning rules for all the six considered combinations are summarized in Table 1. Note that the tuning rules were derived in [1], [16] and [4] for lumped delay position, velocity and acceleration feedback. For the distributed delay case, only acceleration feedback was considered so far in [30]. The velocity and position distributed delay feedback analysis is performed for the first time here. The derivation of the tuning rules is analogous to the acceleration case in [30] and therefore, it is omitted.

In each of the tuning rules corresponding to the lumped delay, we have a single gain value $g_{\cdot}$, but infinitely many possible delay values $\tau_{\cdot l}$, where $l \in \mathbb{N}^+$ denotes a branch number, a counter associated with phase wrap-around (for $\cdot$, a corresponding index used in Table 1 is to be substituted). The proper choice of the delay branch will be addressed in the analysis to follow. In the distributed delay resonator tuning rules, the gain depends on the delay value. In the analysis, the normalized gain $g_{\cdot n} = \frac{g_{\cdot}}{\tau_{\cdot l}}$ is considered, which was also used for derivation of the tuning rules.

Note that certain dependencies can be observed between the parameter values.

Table 1
DR feedback options and its parameters with respect to measurement and delay type

Acceleration, lumped delay	Acceleration, distributed delay
$u(t) = g_a \ddot{x}_a(t - \tau_{al})$ (27)	$u(t) = g_{\bar{a}} \frac{1}{\tau_{\bar{a}l}} \int_0^{\tau_{\bar{a}l}} \ddot{x}_a(t-\theta)d\theta$ (30)
$\tau_{al} = \frac{1}{\omega}\text{atan}\left(\frac{2\zeta\omega}{\omega^2-1}\right) + \frac{2(l-1)\pi}{\omega}$ (28)	$\tau_{\bar{a}l} = \frac{2}{\omega}\text{atan}\left(\frac{2\zeta\omega}{\omega^2-1}\right) + \frac{2(l-1)\pi}{\omega}$ (31)
$g_a = \frac{1}{\omega^2}\sqrt{(\omega^2-1)^2 + 4\zeta^2\omega^2}$ (29)	$g_{\bar{a}} = \tau_{\bar{a}l} \frac{(\omega^2-1)^2+4\zeta^2\omega^2}{4\zeta\omega^2}$ (32)
Velocity, lumped delay	Velocity, distributed delay
$u(t) = g_v \dot{x}_a(t - \tau_{vl})$ (33)	$u(t) = g_{\bar{v}} \frac{1}{\tau_{\bar{v}l}} \int_0^{\tau_{\bar{v}l}} \dot{x}_a(t-\theta)d\theta$ (36)
$\tau_{vl} = \frac{1}{\omega}\text{atan}\left(\frac{1-\omega^2}{2\zeta\omega}\right) + \frac{2(l-1)\pi}{\omega}$ (34)	$\tau_{\bar{v}l} = \frac{2}{\omega}\text{atan}\left(\frac{1-\omega^2}{2\zeta\omega}\right) + \frac{2(l-1)\pi}{\omega}$ (37)
$g_v = \frac{1}{\omega}\sqrt{(\omega^2-1)^2 + 4\zeta^2\omega^2}$ (35)	$g_{\bar{v}} = -\tau_{\bar{v}l} \frac{(\omega^2-1)^2+4\zeta^2\omega^2}{2(\omega^2-1)}$ (38)
Position, lumped delay	Position, distributed delay
$u(t) = g_p x_a(t - \tau_{pl})$ (39)	$u(t) = g_{\bar{p}} \frac{1}{\tau_{\bar{p}l}} \int_0^{\tau_{\bar{p}l}} x_a(t-\theta)d\theta$ (42)
$\tau_{pl} = \frac{1}{\omega}\text{atan}\left(\frac{2\zeta\omega}{\omega^2-1}\right) + \frac{2(l-1)\pi}{\omega}$ (40)	$\tau_{\bar{p}l} = \frac{2}{\omega}\text{atan}\left(\frac{2\zeta\omega}{\omega^2-1}\right) + \frac{2(l-1)\pi}{\omega}$ (43)
$g_p = -\sqrt{(\omega^2-1)^2 + 4\zeta^2\omega^2}$ (41)	$g_{\bar{p}} = -\tau_{\bar{p}l} \frac{(\omega^2-1)^2+4\zeta^2\omega^2}{4\zeta}$ (44)

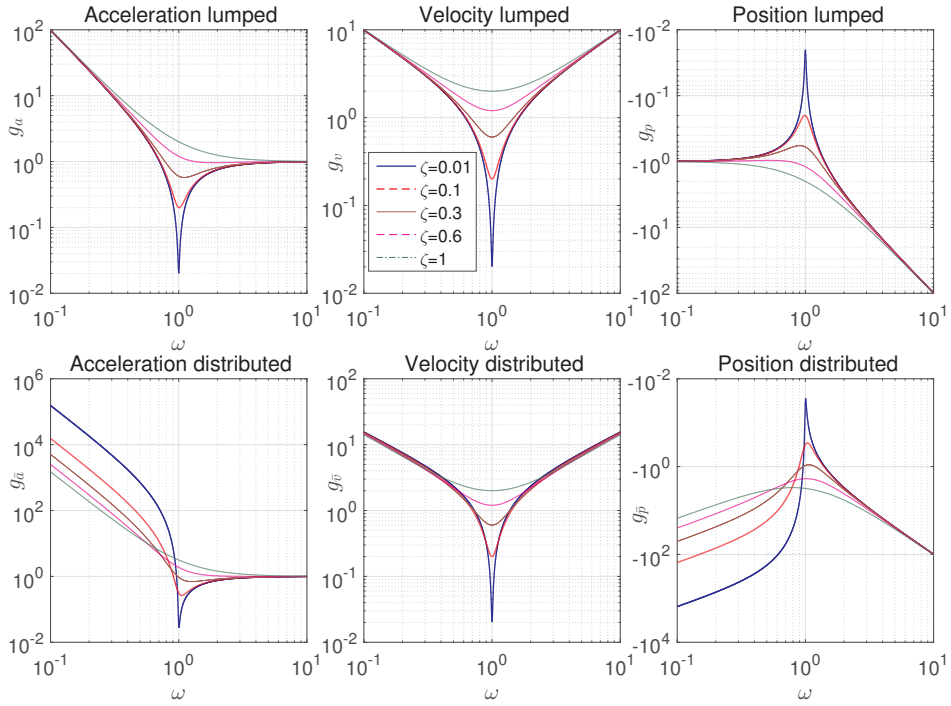

Fig. 3. Gain parameters of active DR feedback ((27), (30), (33), (36), (39) and (42)) with various tuning rules given in Tab. 1. The gains for the distributed delay DR are shown for the first branch ($l = 1$) of the delay.

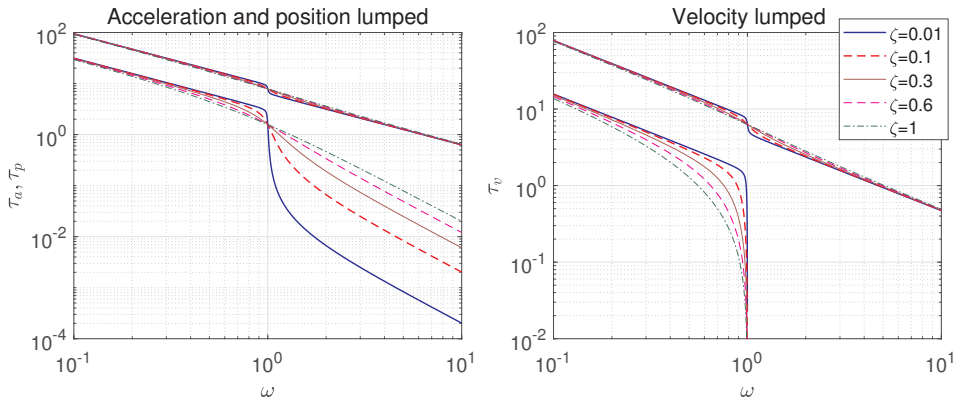

Fig. 4. Delay parameters of active DR feedback ((27), (33) and (39)) with lumped delay according to feedback tuning rules given in Tab. 1, considering the first ($l = 1$ lower set of curves) and the second ($l = 2$ upper set of curves) branches of the delays.

The gain values are related in both the lumped delay

$$-g_p = \omega g_v = \omega^2 g_a \tag{45}$$

and distributed delay

$$-\frac{g_{\bar{p}}}{\tau_{\bar{p}l}} = \frac{2\zeta}{1-\omega^2}\frac{g_{\bar{v}}}{\tau_{\bar{v}l}} = \omega^2 \frac{g_{\bar{a}}}{\tau_{\bar{a}l}} \tag{46}$$

cases. The gain parameters with respect to ω are shown in Fig. 3. Notice that for the distributed delay, the minimal gain sets achieved for $l = 1$ are shown. For all the feedback types, the minimum of the gain magnitude takes place around the absorber resonant frequency $\omega = 1$, considering the preferred lower values of ζ. Note that due to the noise amplification, lower values of the gain should be preferred for the practical implementation. From this point of view, all the DRs perform the best in a narrow range close to $\omega = 1$. For the suppression in the higher frequency range, the acceleration feedback, either lumped or distributed (with $l = 1$), should be preferred due to $g_{a(\bar{a})} \to 1$ as $\omega \to \infty$. On the other hand, the best option for the low frequency range is to be the position lumped delay DR, for which $g_p \to -1$ as $\omega \to 0$.

Even stronger dependencies appear for the delay values, where the delays are identical in position and acceleration feedback

$$\tau_{a1} = \tau_{p1}, \tau_{\bar{a}1} = \tau_{\bar{p}1}, \tag{47}$$

while it is smaller for the velocity feedback

$$\tau_{v1} = \tau_{a1} - \frac{\pi}{2\omega}, \tau_{\bar{v}1} = \tau_{\bar{a}1} - \frac{\pi}{\omega}. \tag{48}$$

Besides, the distributed delay with $l = 1$ is always twice as long as the cor-

responding lumped delay. Therefore only two graphs are presented to demonstrate the delay ranges in Fig. 4 for the branches $l = 1, 2$. Notice also that for the velocity feedback, the first delay branch ($l = 1$) can be used only for $\omega < 1$, because the delay τ_{v1} is negative for the upper frequency range.

It can be seen in the left part of Fig. 4 that the decay rate of the delay with respect to growing frequency is considerably high for the acceleration and position feedback considering $l = 1$ and $\omega > 1$. This can eventually bring delay implementation difficulties at the physical controller considering the requirement $\Delta t << \tau$ on the delay discretization, where Δt is a sampling period. It applies especially for small values of ζ, for which the resulting delays are the smallest. It can also be seen from the left part of Fig. 4 that the second branch of the delays in acceleration and position feedback may seem advantageous for the higher frequency range ($\omega > 1$). Asymptotically, it faces a decay rate of one decade of delay per one decade of frequency. For the first branch of the delay and high frequency range, the asymptotic decay rate is much faster - two decades of delay per one decade of frequency. This lower decay rate for $l = 2$ is due to the term $\frac{2(l-1)\pi}{\omega}$ in the formulas for the delays in Table 1 as it becomes a dominant term in the decay rate for $\omega >> 1$. In fact, the same decay rate applies also for higher branches. At the end, however, it is the first part of each of the delay terms by which the synchronization of the control force with the excitation force is performed. The term $\frac{2(l-1)\pi}{\omega}$ just delays the control force by $l - 1$ periods. Thus, the sampling period to implement the delay needs to be determined with respect to the first delay branch.

5 Robustness and stability analysis

In the next step of the cross-comparison of the set of DR feedback rules, the stability and robustness in vibration suppression with respect to the excitation frequency ω and absorber damping ζ will be studied and presented in form of parametric maps.

In order to analyse the robustness in vibration suppression against the mismatch between the design and true excitation frequency, the *normalized transmissibility function* defined as

$$T(\varpi) = \left| \frac{R(j\varpi) - P(j\varpi)}{Q(j\varpi)} \right| \tag{49}$$

is analyzed, where ϖ is the frequency, which in general can differ from the nominal excitation frequency ω. Note that by coupling equation (4) with the resonator feedback, the transmissibility can be interpreted as $T(\varpi) = \frac{1}{|G_{x_a,x_p}(j\varpi)|}$,

where $G_{x_a,x_p}(s) = \frac{X_a(s)}{X_p(s)}$. By the DR design procedure, it is required that $T(\varpi) = 0$ for the excitation frequency $\varpi = \omega$ implying $|G_{x_p,f}(j\varpi)| = 0$, where the latter transfer function is defined in (7).

In what follows we characterize the robustness of the vibration suppression with respect to deviations of the exciting frequency. Setting $\nu = \varpi/\omega$, where ω and ϖ denote design and true excitation frequencies, we consider the function $\nu \in \mathbb{R} \mapsto h(\nu)$, with

$$h(\nu) = T(\omega\nu).$$

This function satisfies $h(0) = 1$, it is non-negative for all ν and has a zero at $\nu = 1$, corresponding to $\varpi = \omega$. At $\nu = 1$ function h is not differentiable, due to the modulus in (49). However, the limit

$$\kappa := \lim_{\Delta\nu \to 0} \frac{h(1+\Delta\nu)}{|\Delta\nu|}$$

exists (without taking any assumption on the sign of $\Delta\nu$). The value of κ, which we refer to as the *characteristic slope* can be used as a robustness measure of the DR against a frequency mismatch between an external perturbations and the design frequency. Indeed if κ is small (large), then function h has a small (large) directional derivative at $\nu = 1$ in both directions, implying a small / high sensitivity with respect to variations of the frequency to be suppressed. Due to the expression in terms of normalized variable ν the characteristic slope is a relative measure with respect to ω. The following easy-to-compute formula for κ can be readily obtained.

Proposition 3 *The characteristic slope satisfies*

$$\kappa = \omega \frac{|R'(j\omega) - P'(j\omega)|}{|Q(j\omega)|}. \tag{50}$$

Proof. Setting $H(s) = (R(s) - P(s))/Q(s)$ we can express $h(\nu) = |H(j\omega\nu)|$ and obtain

$$\kappa = \omega \left| H'(j\omega) \right|.$$

We have

$$H'(s) = \frac{R'(s) - P'(s)}{Q(s)} - \frac{R(s) - P(s)}{Q(s)^2}.$$

Since $R(j\omega) - P(j\omega) = 0$ from (9), we arrive at

$$H'(j\omega) = \frac{R'(j\omega) - P'(j\omega)}{Q(j\omega)}. \tag{51}$$

Substituting (51) $\kappa = \omega|H'(j\omega)|$ yields (50). □

Thus, if the true excitation frequency ϖ slightly differs from the design exci-

tation frequency ω, e.g. due to inaccuracy of the signal processing unit, the transmissibility magnitude can be estimated by

$$T(\varpi) \approx \kappa \frac{|\varpi - \omega|}{|\omega|}. \tag{52}$$

For derivation of the stability maps, the procedures proposed in [29] and [30] for DRs with acceleration delayed feedback are applied. The analysis is performed with respect to the damping ratio ζ, which (after normalization) is the only physical parameter of the absorber, and the excitation frequency ω. As we have seen in Section 4, these two parameters determine the values of the feedback gain g and delay τ. Thus, the task is to determine the regions in the $\omega \times \zeta$ space, for which the resonator is stable, i.e. the non-assigned roots of (9) are in the open left half plane. These results then can be visualized in the form of stability maps. The maps are determined by applying the Cluster Treatment of Characteristic Roots (CTCR) [31, 32] under frequency sweeping. The methodology, generalized for various resonator types is given in the Appendix.

In what follows, for each of the feedback type, the stability and robustness maps are given and discussed. Even though the stability analysis of DRs with acceleration feedback was done in [29] and [30], the key aspects are recalled for sake of completeness. The robustness analysis is performed for the first time for all the resonator feedback types.

5.1 Acceleration feedback

The stability regions of the DR with acceleration lumped delay feedback (27) derived in [29] are shown in Fig. 5. As can be seen, the largest stability region is achieved for the shortest possible delay τ_{a1}, which is in fact unlimited in the ω direction from the above. With increasing l, the upper stability bound appears and the width of stable frequency range decreases for any damping ζ. Note also that the stability regions are limited with respect to the damping ζ. Thus, from the stability perspective, the branch $l = 1$ should be preferred with the absorber damping close to $\zeta = 0.1$, for which the lower stability bound is minimal.

For the DR with acceleration distributed delay feedback (30) the maps derived in [29] are shown in Fig. 5. Analogously to the lumped delay case, the largest stability region (unlimited from the above) is achieved for $l = 1$. The width of the stable frequency ranges decreases dramatically with increasing l. Interestingly, the stable frequency range gets wider with increasing ζ. Also for this case, from the stability perspective, the shortest possible delay $\tau_{\bar{a}1}$

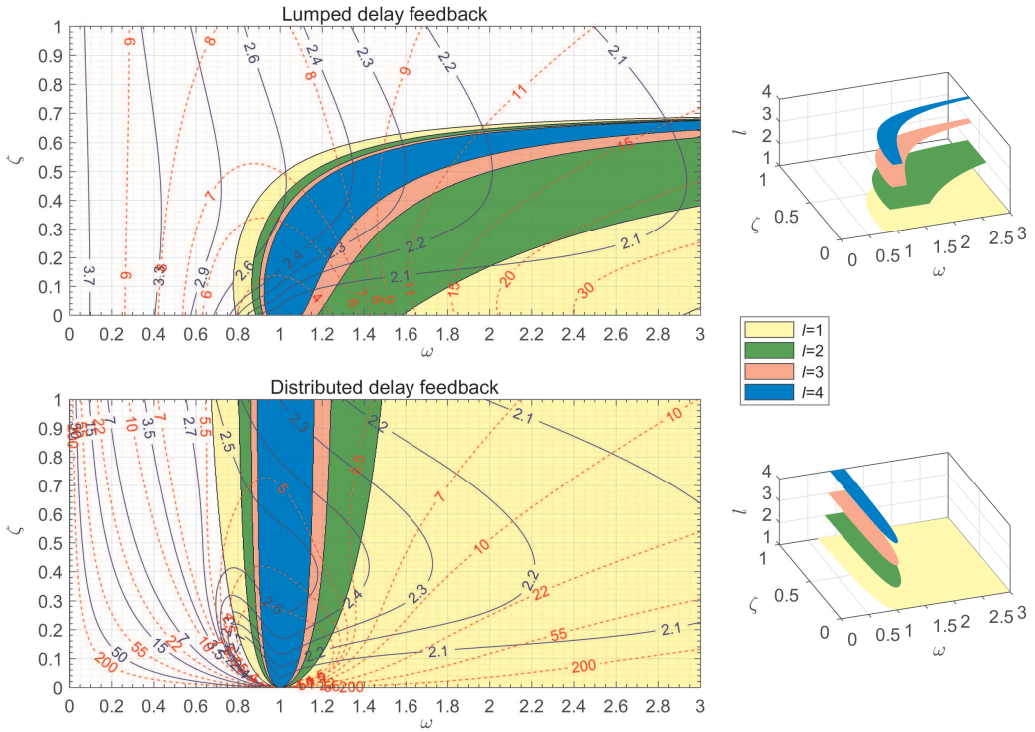

Fig. 5. Stability regions of the DR with acceleration lumped delay feedback (27), and the DR with acceleration distributed delay feedback (30). The contours show the *characteristic slope* κ given by (50), for $l = 1$ (solid) and $l = 2$ (dashed)

is preferred. However, compared to the lumped delay rule, an absorber with rather larger damping should be preferred if the stability width is the primary requirement.

In order to analyze the robustness in vibration suppression, the *characteristic slope* is derived by (50) for $l = 1, 2$ and visualized in both the maps in Fig. 5 as contour lines. For $l = 1$ a relatively small variation of the slope can be observed over the stable regions for both the cases. This is not the case for $l = 2$, where the growth with increasing ω is considerably higher.

Thus, from both the stability and robustness points of view, the setting with $l = 1$ should be preferred. The performance of both acceleration feedback types is more or less equivalent. As a consequence, the distributed delay case should be preferred due to its noise filtering property, which is substantial for the acceleration feedback. This feedback type is also preferred due to retarded character of DR spectrum, as discussed in [30].

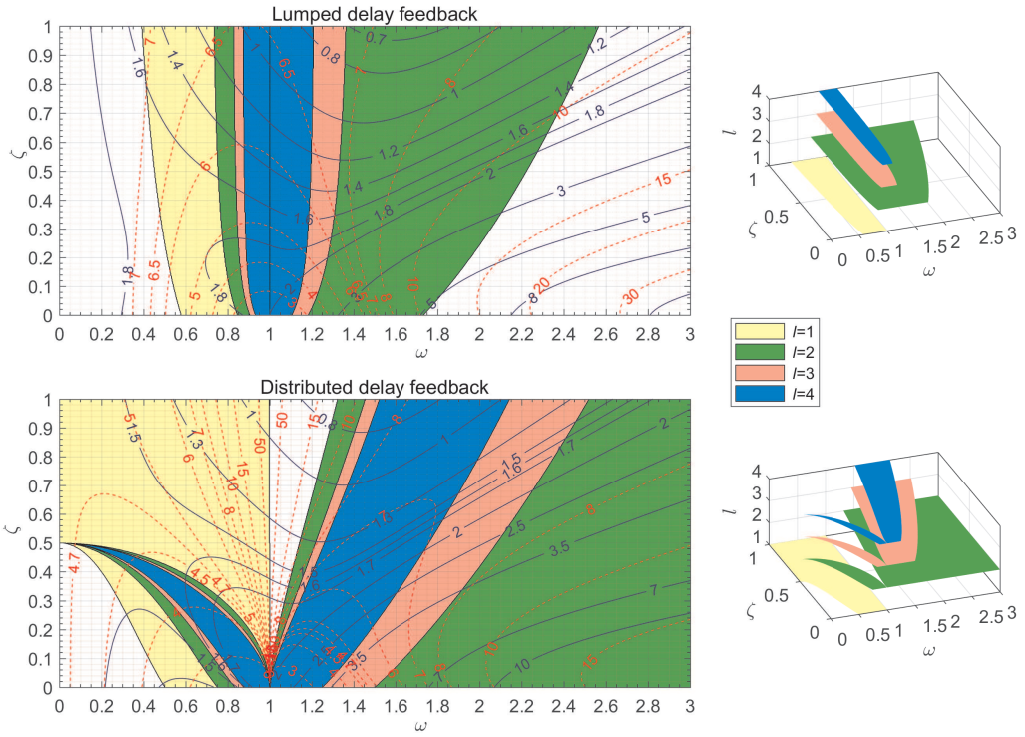

Fig. 6. Stability regions of the DR with velocity lumped delay feedback (33), and the DR with velocity distributed delay feedback (36). The contours show the *characteristic slope* κ given by (50), for $l = 1$ (solid) and $l = 2$ (dashed)

5.2 Velocity feedback

The stability and robustness maps for velocity feedback types (33) and (36) are shown in Fig. 6. For the lumped delay DR with $l = 1$ and $\omega = 1$, the delay $\tau_{vl} = 0$ (and $g_{vl} = 2\zeta$) implies that the feedback simply eliminates the dissipative damping effect for non-delayed case. This frequency determines the upper stability boundary. For $\omega > 1$, only higher branches of the delay values can be considered. As can be seen, the widest range is obtained for $l = 2$. On the other hand, the left stability boundary is the lowest for $l = 1$.

An interesting property of the distributed delay DR with $l = 1$, for which the stability is also bounded by $\omega = 1$, is that for $\zeta > 0.5$, the lower stability bound is $\omega_{s,min} = 0$. For $l = 2$, the stability range is unlimited from above in the considered frequency range. A limiting factor of the distributed delay DR application is instability in the neighborhood of $\omega = 1$ for all the considered delay branches.

Concerning the *characteristic slope*, notice that for both types of delays, it is slightly lower for $l = 1$ over the corresponding stability region when compared to both the acceleration feedback cases. However, for $\omega > 1$, the application

of velocity feedback is inconvenient, as a much higher slope is achieved for the required delay branch $l = 2$, implying a lower robustness in vibration suppression.

Let us remark that the velocity feedback of the form

$$u(t) = \frac{g_{\bar{a}}}{\tau_{\bar{a}l}} \left(\dot{x}_a(t) - \dot{x}_a \left(t - \tau_{\bar{a}l} \right) \right) \tag{53}$$

with the tuning rules (31) and (32) is *formally* identical with the DR with acceleration distributed delay feedback (30). The stability and robustness maps for DR with (53) is then identical to the map in Fig. 5.

Balancing all the features, the instability close to $\omega = 1$ in particular renders both the lumped and distributed delay velocity feedback types impractical. Interestingly, if the velocity sensor is available, the best results are achieved for the feedback form (53), which is practically analogous to the acceleration distributed delay feedback (30), except the lack of noise filtration. Due to a practically unbounded frequency rage from below for $\zeta > 0.5$, the distributed delay DR is well applicable for suppressing low frequency vibrations. However, referring to the force and energy demand analysis performed in Section 3, this solution would require a high force amplitude and a high energy supply.

5.3 Position feedback

The stability map for position feedback with classical delay in Fig. 7 show interestingly a wide area of stability for branch $l = 1$, which covers the full frequency range for $\zeta > 0.71$ and full damping range for $\omega > 0.63$. The stability range for higher branch number gets very narrow and only covers a small area around the natural frequency of the absorber, considering low values of damping ζ.

The stability regions for the distributed delay DR shown in Fig. 7 have similar shapes to the lumped delay DR, just being even smaller for $l > 1$. For $l = 1$ the stability region is also very wide, but the lower bound is higher compared to the lumped delay case for $\zeta < 0.71$. From the *characteristic slope* contours, it can be seen in both the DRs that it is relatively large even for $l = 1$ at the higher frequency range.

Note that analogously to the case of velocity feedback, position feedback of the form

$$u(t) = \frac{g_{\bar{v}}}{\tau_{\bar{v}l}} \left(x_a(t) - x_a \left(t - \tau_{\bar{v}l} \right) \right) \tag{54}$$

with the tuning rules (37) and (38) is *formally* identical with the DR with velocity distributed delay feedback (30). The stability and robustness map for

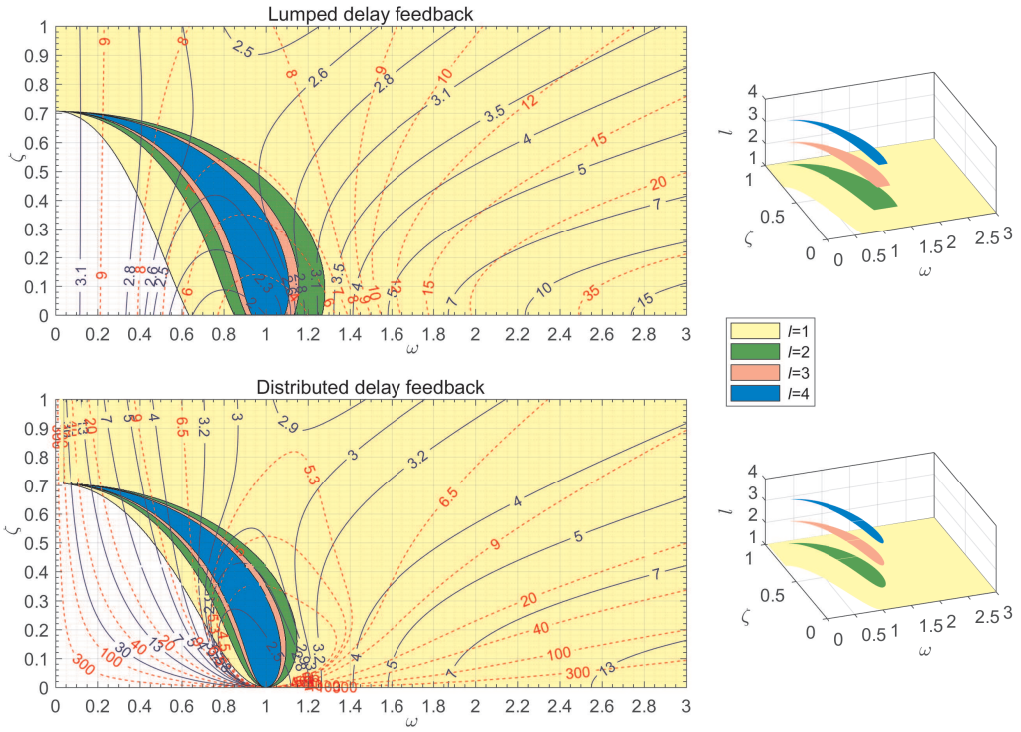

Fig. 7. Stability regions of the DR with position lumped delay feedback (39) and the DR with position distributed delay feedback (42). The contours show the *characteristic slope* κ given by (50), for $l = 1$ (solid) and $l = 2$ (dashed)

DR with (53) is then identical to the map in Fig. 6.

To conclude, the application of position feedback is practical on the lower frequency range, in contrast to acceleration feedback. Due to the high growth of the gain value with decreasing frequency for the distributed delay case shown in Fig. 3, the lumped delay feedback should be preferred.

6 Implications for the active absorber design

For the absorber and the force actuator design, let the design parameters be transferred from the dimensionless to the dimensional form. Starting with the resonator parameters, we obtain

$$\bar{\tau} = \frac{1}{\Omega}\tau \tag{55}$$

and

$$\bar{g} = m_a \Omega^q g \tag{56}$$

where g and τ are dimensionless gain and the delay given in Tab. 1, $q = 2$ for acceleration, $q = 1$ for velocity and $q = 0$ for position feedback.

Considering the relation between the excitation force amplitude F[m] used for the analysis and the true excitation force amplitude $\bar{F}$[N] given by

$$\bar{F} = m_a \Omega^2 F, \tag{57}$$

the rules for the force amplitude (14) peak and absorber position amplitude (18) can be turned to

$$\bar{U} = \frac{\bar{F}}{\bar{\omega}^2} \sqrt{(\Omega^2 - \bar{\omega}^2)^2 + 4\zeta^2 \Omega^2 \bar{\omega}^2} \tag{58}$$

and

$$X_a = \frac{\bar{F}}{m_a \bar{\omega}^2}, \tag{59}$$

respectively. The exerted power $\bar{P}$[W] is linked with P[m^2] used in the analysis above by the relation

$$\bar{P} = m_a \Omega^3 P. \tag{60}$$

Thus, by (57) and (60), the power supply relation (21) is turned to

$$\bar{P}_{\max} = \frac{\zeta \Omega \bar{F}^2}{m_a \bar{\omega}^2} + \frac{\bar{F}^2}{2 m_a \bar{\omega}^3} \sqrt{(\Omega^2 - \bar{\omega}^2)^2 + 4\zeta^2 \Omega^2 \bar{\omega}^2} \tag{61}$$

where the first term corresponds to the averaged power supply $\bar{P}_{av}$.

From the above derived rules, except the force amplitude (58), the delayed resonator performance characteristics highly depend on the absorber mass m_a, next to Ω and ζ. The following design rule is motivated by minimizing the mass dependent characteristics such as position deflection (59), power supply (61) (including the $\bar{P}_{av}$ part):

- **Design rule 1**: the *absorber mass* m_a is to be selected as large as possible, taking into account the construction constraints of the overall set-up.

Taking into consideration the system structure in Fig. 1, a reasonable upper bound on the absorber mass is the mass of the main body m_p, i.e. $m_a < m_p$. As a rule, however, it is considerably smaller. For selecting its proper value, various aspects need to be taken into account, such as maximal amplitude of the excitation force $\bar{F}_{max}$ and available space for the absorber motion, discussed below.

When designing the active resonator absorber, the *fundamental input parameters* are:

(1) the operable frequency range $[\bar{\omega}_{\min}, \bar{\omega}_{\max}]$

(2) the maximum excitation force amplitude profile $\bar{F}_{\max}(\bar{\omega})$.

Directly from (59), the second design rule is obtained for determining the absorber position deflection:

- **Design rule 2**: the *maximum absorber position amplitude* determining the position deflection range $x_a \in [-X_{a\max}, X_{a\max}]$ of the absorber actuator is given by

$$X_{a\max} = \frac{1}{m_a} \max \left\{ \frac{\bar{F}_{\max}(\bar{\omega})}{\bar{\omega}^2} \right\}, \tag{62}$$

  with $\bar{\omega} \in [\bar{\omega}_{\min}, \bar{\omega}_{\max}]$.

The design of the other two absorber characteristics Ω and ζ, together with m_a determining the stiffness and damping k_a, c_a of the absorber (1), is a multi-objective optimization task. Concerning the force amplitude and energy demands, see Fig. 2, the best performance is achieved for small values of the damping ζ and for $\bar{\omega} \approx \Omega$. However, the risky feature of small damping ζ is the requirement of a high sampling rate due to steep decay of the delay for increasing frequency on the range $\bar{\omega} > \Omega$, considering the preferred delay branch $l = 1$ and acceleration or position feedback, see Fig. 4. On the other hand when the excitation frequency decreases in the range $\bar{\omega} < \Omega$, the force amplitude tends to increase substantially. The additional constraints on ζ and Ω comes from the required stability of the resonator and robustness characteristics over the given frequency range, which depend on the sensor type, as shown in the maps in Figs. 5, 6 and 7 and discussed above. Balancing all these properties and constraints, the final design rule can be formulated as follows:

- **Design rule 3**: The *natural frequency* Ω is to be placed within the range $[\bar{\omega}_{\min}, \bar{\omega}_{\max}]$ and the *damping* ζ is to be selected so that the resonator is stable over the whole range for the given feedback type. Note that the closer Ω to $\bar{\omega}_{\min}$ is, the lower is the delay value τ for the upper frequency point $\bar{\omega}_{\max}$, which can be undesirable due to a high sampling rate requirement imposed by the delay implementation constraint $\tau >> \Delta t$, where Δt is the sampling period. On the other hand, the closer Ω is to $\bar{\omega}_{\max}$, the higher is the force amplitude needed for suppressing vibrations at $\bar{\omega}_{\min}$. Small values of ζ are to be preferred with respect to less energy demand, unless the stability constraints and active feedback sampling rate do not impose a preference for larger values of ζ. Furthermore, small ζ is also preferable in the sense of robustness for acceleration and position feedbacks when Ω is selected around nominal excitation frequency.

7 Conclusions

A complete analysis of delayed resonators with acceleration, velocity and position feedback, considering both lumped and distributed delay, was performed. From the analysis of the stability and robustness, it results that the first delay branch ($l = 1$) should be preferred in all the architectures. For the acceleration feedback, assuming the delay τ_1 and rather smaller values of the damping ($\zeta < 0.3$, preferred due to power supply demands), the performance of both delay alternatives is more or less equivalent from the stability and robustness points of view. Thus, the distributed delay feedback should be preferred due to its noise filtering feature. It also results from the analysis that this feedback type is to be preferred rather for the high frequency vibration suppression. An advantage of this architecture is the easy implementation by deploying the accelerometer sensors, which are of relatively low cost compared to position and velocity sensors.

An impractical aspect of velocity feedback is the limited operable frequency range for the $l = 1$ delay branch, which is bounded from above by the natural frequency Ω of the absorber. For the higher frequency range, the delay branch $l = 2$ is to be used, for which the robustness in vibration suppression decreases considerably. Besides, operating the absorber in the range $\bar{\omega} < \Omega$ is impractical due to high force amplitude and power supply demands. Thus when the velocity sensor is available, the feedback of the form (53) is to be preferred, which is formally identical with the acceleration feedback with distributed delay and takes over its favorable characteristics, except the noise filtration feature.

Considering the position feedback, it features analogous characteristics as the acceleration feedback. The key difference is in the relatively high *characteristic slope* in the higher frequency range indicating a lower robustness level compared to the acceleration feedback. On the other hand, particularly for the lumped delay, the stability region has a lower stability boundary compared to acceleration feedback. Thus, the application of position feedback is practical on the lower frequency range compared to acceleration feedback. In this case, however, the lumped delay feedback should be preferred as it requires considerably lower gain in the low frequency range, as shown in Fig. 3.

Next to the analysis of the various DR architecture performed for the dimensionless parameter model, the implications for the absorber and the actuator design have been addressed. As the main result, three *design rules* have been proposed in Section 6. The first two, targeting the absorber mass and its position deflection range, are straightforward to apply. On the other hand, the selection of the absorber natural frequency and the damping is a multi-criteria task, where the operable range of frequencies, the stability range depending

on the feedback structure, the available maximum force amplitude by the actuator, energy considerations and minimal delay implementation are to be balanced. However, all these aspects have been addressed in this paper and it is an end-user task to weight them when forming the design objective function.

8 APPENDIX - Determining the stability maps by CTCR method and frequency sweeping

Consider the resonator (2) and the general DR feedback determined by the transfer function (24), where the transfer function depends on the two parameters g and τ by which a root couple is placed at $\pm j\omega$. For the analysis, however, the delay parameter is left to be independent of the frequency ω. This leads to the analysis of the following characteristic equation with dimensionless parameters

$$M\left(s,\ \vartheta\right) = s^2 + 2\zeta s + 1 - P(s, g, \vartheta), \tag{63}$$

where $0 \leq \vartheta$ is the independent delay. This is done with the objective to identify systematically all the delay values ϑ for the given gain g for which the root appears at, and subsequently crosses, the imaginary axis. Starting from $\vartheta = 0$ for which the stability posture is known, identifying the root crossings for gradually increasing ϑ, the number of rightmost roots can be determined by CTCR for any delay value ϑ. Thus, to determine whether the DR is stable for a given values g and τ, all the values of $\vartheta \in [0, \tau]$ for which (63) has imaginary roots need be detected. The characteristic equation of a single delay system, evaluated on the imaginary axis, can be interpreted as an equation in two independent variables $j\omega \in j\mathbb{R}$ and z on the complex unit circle, where the relation with the original equation is given by $z = e^{-j\omega\tau}$. The CTCR can then be interpreted as an approach based on substitution of the variable z. Alternative approaches are based on eliminating one of the two variables, leading to a (generalized) eigenvalue problem in the other variable (elimination of z in [33] , elimination of $j\omega$ in the matrix pencil approach [34]), or by frequency sweeping [35].

The core of CTCR procedure [31], [32], lies in the application of the Rekasius substitution [36]

$$e^{-\vartheta s} \rightarrow \frac{1 - Ts}{1 + Ts}. \tag{64}$$

which is exact for $s = j\bar{\omega}$, $\bar{\omega} \in R^+$ with the correspondence between T and ϑ

$$\vartheta = \frac{2}{\bar{\omega}} \left[\tan^{-1}\left(\bar{\omega}T\right)\ + k\pi\right], \quad k \in \mathbb{N}^+. \tag{65}$$

Deploying (64) in equation (63) and multiplying the equation by $1 + Ts$, the

Table 2
Routh's array for (66)

s^3	$H_3(g,T)$	$H_1(g,T)$
s^2	$H_2(g,T)$	$H_0(g,T)$
s^1	$R_1(T) = \frac{H_2(g,T)H_1(g,T) - H_3(g,T)H_0(g,T)}{H_2(g,T)}$	
s^0	$H_0(g,T)$	

characteristic equation is brought to the form

$$H_3(g,T)s^3 + H_2(g,T)s^2 + H_1(g,T)s + H_0(g,T) = 0. \tag{66}$$

The roots of this cubic equation have no relation with those of (63) except when the roots are imaginary. This however matches the goal of the analysis, which is to determine the values of ϑ or corresponding T for which the roots are imaginary. For this purpose, the corresponding Routh's array to equation (66) given in Table 2 is constructed as suggested in [31], [32]. The equation (66) has roots on the imaginary axis if $R_1(T) = 0$ from Table 2, and the auxiliary equation

$$H_2(g,T)s^2 + H_0(g,T) = 0 \tag{67}$$

returns the corresponding imaginary roots $s_{1,2} = \pm j\bar{\omega}$, with

$$\bar{\omega} = \sqrt{\frac{H_0(g,T)}{H_2(g,T)}} \tag{68}$$

if $H_2(g,T)H_0(g,T) > 0$. The equality condition $R_1(T) = 0$ results in

$$H_2(g,T)H_1(g,T) - H_3(g,T)H_0(g,T) = 0, \tag{69}$$

which provides at most two real values $T_{1,2}$. The corresponding imaginary roots of (66) are determined from (68). Thus, for each value of $T_p,\ p = 1, 2$, a root crossing frequency $\bar{\omega}_p$ given by (68) exists, if the given inequality conditions are satisfied. From (65), the corresponding delay values for these imaginary roots are found

$$\vartheta_{p,k} = \frac{2}{\bar{\omega}_p}\left[\tan^{-1}(\bar{\omega}_p T_p)\ + (k-1)\pi\right], \quad k = 1, 2, \ldots. \tag{70}$$

As an important step of CTCR, the root tendency

$$RT\left(\bar{\omega}_p, \vartheta_{p,k}\right) = \operatorname{sign}\left\{\left[\left.\frac{\partial s}{\partial \vartheta}\right|_{\substack{s=j\bar{\omega}_p \\ \vartheta=\vartheta_{p,k}}}\right]\right\} \tag{71}$$

is determined to decide whether the root crossing is stabilizing, $RT\left(\bar{\omega}_p, \vartheta_{p,k}\right) = -1$, or destabilizing, $RT\left(\bar{\omega}_p, \vartheta_{p,k}\right) = 1$. This is investigated through

$$\frac{\partial s}{\partial \vartheta} = \frac{\frac{\partial M(s,\vartheta)}{\partial \vartheta}}{\frac{\partial M(s,\vartheta)}{\partial s}} \tag{72}$$

for $s = j\bar{\omega}_p$ and $\vartheta = \vartheta_{p,k}$, p=1,2.

Assuming the damping parameter ζ is fixed, the above CTCR procedure can be applied for determining the values of ϑ, for which the DR has roots on the imaginary axis. Subsequently, knowing the root tendency at the given frequency point, the number of unstable roots can be determined for any value of ϑ. Let us note that for a given g which is determined for a given excitation frequency ω we may have two values of $T_{1,2}$. By the synthesis, one of them $T_{1(2)}$ will correspond to the design value $\vartheta_{1(2)} = \tau$, including its infinitely many branches, yielding the design crossing frequency ω by (68). The other value $T_{2(1)}$ then provides a value of the other delay $\vartheta_{2(1)}$, and its corresponding branches, which results in a root at a different frequency than ω (except the degenerative cases when $\vartheta_1 = \vartheta_2$). The knowledge of this other delay is irrelevant from the DR design point of view, but is crucial for determining the stability maps. The stability maps are determined by application of the following two algorithms.

Algorithm 1 - determining stable frequency range
Assume the parameter ζ is fixed, the excitation frequency range $\omega \in [\omega_{s,\min}, \omega_{s,\max}]$ for which the DR forms an ideal stable resonator can be determined as follows:

(1) Cover the excitation frequency range of interest by a sufficiently dense grid. For each grid point ω_i, determine the value of g_i by the corresponding DR design formula. After this, the delay ϑ is the only free parameter of the characteristic equation (63).
(2) For each grid value with a fixed gain g_i, apply the CTCR procedure to the characteristic equation (63) and determine values $\vartheta_{p,k}$, ($p = 1, 2$ and $k = 0, 1, 2, ...$ denoting the branch points), corresponding frequency (one of which is identical with given ω_i point) and root tendency $RT(\omega_p, \vartheta_{p,k})$ for each of the two delay values. Due to the root continuity with respect to small changes of parameters, after sweeping the excitation frequency

over all the grid points, this procedure will form set of curves in the $\omega \times \vartheta$ coordinates.

(3) For a given ω_i, determine the number of unstable roots NU for $\vartheta = 0$, i.e. for delay free system with only two roots.

(4) Gradually increase ϑ at the given ω_i and count NU roots when passing the curves corresponding to $\vartheta_{p,k}$. Recall that at this curve, we have a root at the imaginary axis and RT determines the direction at which the root moves when ϑ is slightly increased. Thus, if $RT = 1$, NU is increased by one and if $RT = -1$, NU is decreased by one.

(5) For this frequency point ω_i, the delay values τ (and its corresponding branch points) resulting in stable DR, is given by the values of $\vartheta_{p,k}$ for which $\pm j\omega_i$ is the rightmost couple of roots for given g_i, i.e. $NU = 0$. Due to root continuity, the *stable* values of τ form curves in the space $\omega \times \vartheta$. These curves, however, lie only at a limited frequency range due to the given stability constraint. These frequency ranges $\omega \in (\omega_{s,\min}, \omega_{s,\max})$ are the main result of the algorithm.

For the demonstration of the above algorithm, we refer to [29] and [30], for the resonators with acceleration feedback with lumped and distributed delay. The whole stability map is then determined by the following algorithm.

Algorithm 2 - forming the stability maps

(1) Cover the range $\zeta \in [0,\ 1]$ by a sufficiently dense grid.

(2) Apply the Algorithm 1 for each ζ_i and determine the stable frequency ranges for all the delay τ branches of interest.

(3) For each branch number, form the boundaries of stable region by connecting the boundary frequency points obtained for ζ_{i-1}, ζ_i and ζ_{i+1}, $i = 1, 2, 3....$

Acknowledgement

The presented research has been supported by the Czech Science Foundation under the project 17-20943S, by the project C14/17/072 of the KU Leuven Research Council and by the project G0A5317N of the Research Foundation-Flanders (FWO - Vlaanderen). The work of the third author was supported by the European Regional Development Fund under the project Robotics for Industry 4.0 (reg. no. CZ.02.1.01/0.0/0.0/15_003/0000470).

References

[1] N. Olgac, B. Holm-Hansen, A novel active vibration absorption technique: delayed resonator, Journal of Sound and Vibration 176 (1) (1994) 93–104.

[2] N. Olgac, Delayed resonators as active dynamic absorbers, US Patent 5,431,261 (Jul. 11 1995).

[3] N. Olgac, M. Hosek, Active vibration absorption using delayed resonator with relative position measurement, Journal of Vibration and Acoustics 119 (1) (1997) 131–136.

[4] N. Olgac, H. Elmali, M. Hosek, M. Renzulli, Active vibration control of distributed systems using delayed resonator with acceleration feedback, Journal of Dynamic Systems, Measurement, and Control 119 (3) (1997) 380–389.

[5] N. Olgac, B. Holm-Hansen, Tunable active vibration absorber: the delayed resonator, Journal of Dynamic Systems, Measurement, and Control 117 (4) (1995) 513–519.

[6] N. Olgac, B. Holm-Hansen, Design considerations for delayed-resonator vibration absorbers, Journal of Engineering Mechanics 121 (1) (1995) 80–89.

[7] N. Olgac, Single mass dual frequency fixed delayed resonator, US Patent 5,505,282 (Apr. 9 1996).

[8] N. Olgac, H. Elmali, S. Vijayan, Introduction to the dual frequency fixed delayed resonator, Journal of Sound and Vibration 189 (3) (1996) 355–367.

[9] M. Hosek, H. Elmali, N. Olgac, A tunable torsional vibration absorber: the centrifugal delayed resonator, Journal of Sound and Vibration 205 (2) (1997) 151–165.

[10] M. Hosek, H. Elmali, N. Olgac, Centrifugal delayed resonator pendulum absorber, US Patent 5,934,424 (Aug. 10 1999).

[11] N. Olgac, H. Elmali, Analysis and design of delayed resonator in discrete domain, Journal of Vibration and Control 6 (2) (2000) 273–289.

[12] M. E. Renzulli, R. Ghosh-Roy, N. Olgac, Robust control of the delayed resonator vibration absorber, IEEE Transactions on Control Systems Technology 7 (6) (1999) 683–691.

[13] M. Hosek, N. Olgac, A single-step automatic tuning algorithm for the delayed resonator vibration absorber, IEEE/ASME Transactions on Mechatronics 7 (2) (2002) 245–255.

[14] N. Jalili, N. Olgac, Multiple delayed resonator vibration absorbers for multi-degree-of-freedom mechanical structures, Journal of Sound and Vibration 223 (4) (1999) 567–585.

[15] D. Filipovic, N. Olgac, Torsional delayed resonator with velocity feedback, IEEE/ASME Transactions on Mechatronics 3 (1) (1998) 67–72.

[16] D. Filipović, N. Olgac, Delayed resonator with speed feedback–design and performance analysis, Mechatronics 12 (3) (2002) 393–413.

[17] R. Rana, T. Soong, Parametric study and simplified design of tuned mass dampers, Engineering Structures 20 (3) (1998) 193–204.

[18] G.-L. Lin, C.-C. Lin, B.-C. Chen, T.-T. Soong, Vibration control performance of tuned mass dampers with resettable variable stiffness, Engineering Structures 83 (2015) 187–197.

[19] C. Verbaan, P. Rosielle, M. Steinbuch, Broadband damping of non-rigid-body resonances of planar positioning stages by tuned mass dampers, Mechatronics 24 (6) (2014) 712–723.

[20] A. S. Kammer, N. Olgac, Electromechanical delayed resonator implementation using piezoelectric networks, IFAC-PapersOnLine 49 (10) (2016) 71–76.

[21] N. Olgac, N. Jalili, Modal analysis of flexible beams with delayed resonator vibration absorber: theory and experiments, Journal of Sound and Vibration 218 (2) (1998) 307–331.

[22] N. Alujević, I. Tomac, P. Gardonio, Tuneable vibration absorber using acceleration and displacement feedback, Journal of Sound and Vibration 331 (12) (2012) 2713–2728.

[23] H. Rivaz, R. Rohling, An active dynamic vibration absorber for a hand-held vibro-elastography probe, Journal of Vibration and Acoustics 129 (1) (2007) 101–112.

[24] V. Kučera, D. Pilbauer, T. Vyhlídal, N. Olgac, Extended delayed resonators–design and experimental verification, Mechatronics 41 (2017) 29–44.

[25] D. Pilbauer, T. Vyhlídal, W. Michiels, Optimized design of robust resonator with distributed time-delay, Journal of Sound and Vibration 443 (2018) 576–590.

[26] M. Kuře, T. Vyhlídal, W. Michiels, I. Boussaada, Spectral design of robust delayed resonator by double-root assignment, IFAC-PapersOnLine 51 (14) (2018) 72–77.

[27] O. Eris, A. F. Ergenc, S. Kurtulan, A modified delayed resonator for active suspension systems of railway vehicles, IFAC-PapersOnLine 48 (12) (2015) 281–285.

[28] O. Eris, B. Alikoc, A. F. Ergenc, A new delayed resonator design approach for extended operable frequency range, Journal of Vibration and Acoustics 140 (4) (2018) 041003.

[29] T. Vyhlídal, N. Olgac, V. Kučera, Delayed resonator with acceleration feedback–complete stability analysis by spectral methods and vibration absorber design, Journal of Sound and Vibration 333 (25) (2014) 6781–6795.

[30] D. Pilbauer, T. Vyhlidal, N. Olgac, Delayed resonator with distributed delay in acceleration feedback - design and experimental verification, IEEE/ASME Transactions on Mechatronics 21 (4) (2016) 2120–2131.

[31] N. Olgac, R. Sipahi, A practical method for analyzing the stability of neutral type LTI-time delayed systems, Automatica 40 (5) (2004) 847–853.

[32] N. Olgac, R. Sipahi, The cluster treatment of characteristic roots and the neutral type time-delayed systems, in: ASME 2004 International Mechanical Engineering Congress and Exposition, 2004, pp. 1359–1368.

[33] J. Louisell, Absolute stability in linear delay-differential systems: Ill-posedness and robustness, IEEE transactions on automatic control 40 (7) (1995) 1288–1291.

[34] S.-I. Niculescu, Delay effects on stability: a robust control approach, Vol. 269, Springer Science & Business Media, 2001.

[35] K. Gu, J. Chen, V. L. Kharitonov, Stability of time-delay systems, Springer Science & Business Media, 2003.

[36] Z. Rekasius, A stability test for systems with delays, in: Joint Automatic Control Conference, no. 17 in 1, 1980, p. 39.